

5 Earth's Surface Morphology and Convection in the Mantle

R. W. Griffiths¹ and J. A. Whitehead²

¹ Research School of Earth Sciences, The Australian National University, Canberra 0200 ACT, Australia

² Woods Hole Oceanographic Institution, Woods Hole, MA 02543, USA

5.1 Introduction

It is now generally agreed that the Earth's solid mantle is undergoing thermal convection. Much of the evidence for this conclusion is derived from geological and geophysical observations of the Earth's surface, its relative horizontal motions and its topography. Direct consequences of the mantle flow include plate tectonics, which refers to the relative motions of the continents, spreading of the sea-floor, creation of new crust and mid-ocean ridges at spreading centres, and subduction at ocean trenches, along with associated phenomena such as mountain building and volcanism. The motion of the mantle over geological time scales is driven by gravity acting on density differences, which result from loss of heat from the Earth's surface and, to a lesser extent, from transfer of heat from the Earth's core to the mantle. Mantle convection phenomena are reviewed here in the context of geomorphology because they are responsible for producing much of the large-scale topography (horizontally > 10 km) of the Earth's surface. This topography, in turn, imposes strong influences on the atmosphere and ocean circulation patterns, affects precipitation, and provides the base on which erosion and sedimentation processes act. The surface transport processes can also couple back to mantle flow and topography through redistribution of loading on the mantle.

We briefly introduce the nature of the mantle, the behaviour of convection at large Rayleigh numbers, and the mantle's expected response to boundary heat fluxes. We then outline convective instability of a boundary layer, several forms of large-amplitude plume flows, and the formation and subduction of oceanic lithosphere plates. We conclude with a discussion of the surface topographic expressions of these phenomena. These phenomena are discussed in the context of two main notions: 1) we paint a picture of the mantle as a convecting viscous fluid in which heat lost from the Earth's core drives blobs and continuous streams of fluid to ascend from the core-mantle boundary to the surface as plumes, where they create isolated morphological features such as island chains and flood basalt plateaux; 2) the plumes, however, are relatively minor in the heat budget of the mantle and they ascend through much larger-scale convective flows driven by the cooling of the lithosphere. The surface cooling produces subducting slabs that plummet downward and morphological features such as deep ocean trenches and mid-ocean ridges. The article is concerned with a few of the dynamical

phenomena in the mantle rather than with the geological evidence but it should be recognised that the dynamical modelling discussed here must go hand in hand with a range of observational evidence.

5.2 Some Basic Assumptions and Deductions

Before treating a number of specific problems in thermal convection we consider three basic concepts which, explicitly or implicitly, enter into every physically realistic discussion of convection in the mantle.

5.2.1 The Rheology of the Mantle

Seismic and petrological evidence indicates that the bulk of the mantle is a crystalline solid. However, imposed stresses can produce irreversible deformation or creep. The two ‘flow’ mechanisms considered most relevant to the mantle are ‘diffusion creep’, in which the strain rate is proportional to the stress; and ‘dislocation creep’, in which the strain rate is proportional to a higher power of the stress [20]. Both these behaviours allow arbitrarily large strains, so that solids with these properties have no long-term strength. This ensures that in both cases an “effective viscosity” can be defined for mantle materials on geological timescales (although this “viscosity” depends on the average stress level, if dislocation creep is appropriate). Hence the mantle is treated as a viscous fluid in analytical and numerical models of mantle convection, and laboratory experiments directly relevant for the understanding of mantle dynamics (i.e. properly scaled to duplicate the dynamics of the Earth) can be carried out with linear viscous fluids.

Regardless of the details of the rheology, the effective viscosity is strongly temperature-dependent. Assuming diffusion creep is the mechanism by which deformation is accommodated, the viscosity η will be of the form

$$\eta = \eta_0 \exp(AT_M/T), \quad (5.1)$$

where T_M is the melting temperature and A the activation energy. For a mantle of olivine, $A = 30$ at the pressures of interest and $\eta_0 = 10^9$ Pas ([63] and summarized by [61]). For $\eta = 10^{22}$ Pas (a mean value to order of magnitude inferred from postglacial uplift) [38] $T = 0.77 T_M$ and η changes by an order of magnitude as T/T_M changes by only about 5%. We will see below that this strong dependence of η on temperature ensures that it adjusts to a value which depends on the presence of mantle convection. That is, the value of this material property is determined, through the temperature and within wide bounds set by the microscopic mechanics of the mantle material, by the dynamics and motions of the mantle. This conclusion contrasts with the view that whether or not mantle convection occurs is predetermined by the viscosity. The viscosity will, of course, vary from place to place within the convection system according to the temperature variation, and further studies have considered the additional effects of a probable pressure-dependence of the viscosity [16].

5.2.2 Thermal Forcing and the Inevitability of Convection in the Mantle

The Earth's mantle is bounded above by the oceans and atmosphere, and below by the outer core of liquid metal. The mantle is losing heat from the surface at a rate of approximately 3.5×10^{13} W, mostly through the oceanic crust where the fluxes are between 40 mW m^{-2} through old crust and 100 mW m^{-2} through young crust. This heat originates largely from the radioactive decay of elements distributed throughout the mantle (so called 'internal heating'), with a small but significant component (estimated to be approximately 10% of the total surface heat loss, [17]) entering from the core. The latter flux represents a cooling of the core through geological time and is expected to provide the driving force for the geodynamo (through both thermal and compositional convection, the latter resulting from the cooling and consequent solidification of components of the outer core on to a growing solid inner core [5]).

Following the argument put forward originally by Tozer [62], and restated by Stevenson and Turner [61], we consider the behaviour of the mantle when subjected to a purely vertical temperature gradient, and begin by assuming that the physical properties are uniform. The stability of such a fluid layer, heated from below or cooled from above, is a classic problem in fluid mechanics and we quote only the basic results. The onset of convection in this simplest approximation is governed entirely by the Rayleigh number, Ra , which is essentially the ratio of the driving force (due to thermal buoyancy and influenced by diffusion of heat) to the retarding force (due to diffusion of momentum by viscous stresses). For a fluid layer of depth H , with constant kinematic viscosity $\nu = \eta/\rho$ and thermal diffusivity κ ,

$$Ra = \frac{g\alpha\beta H^4}{\nu\kappa}, \quad (5.2)$$

where g is the acceleration due to gravity, α is the coefficient of thermal expansion, and β is the difference between the actual overall temperature gradient (from top to bottom boundary) and the adiabatic temperature gradient. If Ra exceeds a critical value, Ra_c , of about 10^3 (the exact value depending on the boundary conditions) then convection will occur. For internal heating at a prescribed flux and cooling from the top boundary the relevant Rayleigh number can still be defined as in (5.2), except that β is now the (horizontally averaged) superadiabatic temperature gradient that would be required for a conductive steady state given the imposed rate of heat generation.

Rather than trying to evaluate Ra in the Earth using the poorly known present values of the physical properties (β being a particularly large source of uncertainty), the inevitability of mantle convection can be demonstrated by an idealized thermal evolution calculation based on the strong temperature dependence of viscosity (5.1). Consider again a horizontal layer of thickness H , but now containing a uniformly distributed energy source, representing heating due to decay of radioactive elements. The bottom boundary is supposed to be insulated, and the top temperature is fixed at $T = 0^\circ\text{C}$. At time $t = 0$, we suppose

that the temperature $T = T_0$ everywhere and that subsequently, but before convection occurs, the temperature distribution obeys the diffusion equation (with a source term included) – that is, the heat generated is transported only by conduction.

As discussed in more detail by Stevenson and Turner [61], the scale and conductivity of the Earth are such that the heat generated cannot escape by conduction alone in the age t_E of the Earth. The diffusion lengthscale $l \approx (\kappa t)^{1/2}$ is a few hundred kilometres when $t = t_E$, so that a small body could lose most of its heat by conduction as it is generated. However, the much larger model Earth heats up, developing a temperature profile which is fixed at the surface but with increasing temperature and temperature gradient at all depths. As T increases, η given by (5.1) rapidly decreases, and a time is inevitably reached when Ra over some depth interval exceeds the critical value for convection to occur, virtually whatever the magnitude of the temperature gradient. The subsequent behaviour is for all regions eventually to become convective (except possibly the outermost highly viscous layer, which is a boundary layer and will be discussed in more detail below). This follows from the fact that any non-convecting region must continue to heat up, because conduction is too small to remove the heat generated, and so it must achieve a progressively lower viscosity until it takes part in the convection. Given the large depth of the mantle and the expected values of the constants in (5.1) and (5.2), a small enough viscosity is achieved at subsolidus temperatures for convective heat transport to become possible before melting occurs at any depth.

5.2.3 Boundary Layers in Convection at High Rayleigh Numbers

The above argument concentrates on the initiation of convection in the interior of a progressively heated mantle. It is clear that the eventual steady state must have a much larger heat transport than can be achieved by conduction, and that the corresponding Rayleigh number will be much greater than the critical value.

Two other points are useful in understanding the finite amplitude flow in the earth's mantle. The viscosity ν is very large, effectively infinite, relative to the thermal diffusivity κ (i.e. infinite Prandtl number $Pr = \nu/\kappa$), and so the viscous response to a perturbation is instantaneous relative to the thermal response. Secondly, for large Rayleigh numbers the convective heat transport is much more important than conductive heat transport over most of the depth (the ratio $uH/\kappa \approx 10^3$, where u is a typical flow velocity such as that of the tectonic plates). Conduction remains important, however, in thin boundary layers through which heat is transported to and from the interior, and which in fact determine the magnitude of the flux which must be carried by the convection in the interior.

Some fundamental predictions can be made on the basis of dimensional reasoning, as follows. Suppose that the flux does depend only on the material properties and on conditions very near the boundaries, i.e. that it is independent of the total depth H . It follows from their definitions that the Nusselt number Nu , the ratio of the actual heat flux to the purely conductive flux down a linear (super-adiabatic) temperature gradient between the two boundaries, and the

Rayleigh number are related by:

$$Nu = cRa^{1/3}, \quad (5.3)$$

since this is the only form which gives a flux independent of H . The constant $c \approx 0.1$ but can depend on the boundary conditions. A phenomenological theory due to Howard [36] suggests that the conductive boundary layer is inherently unsteady, with cold (or hot) material breaking away intermittently. The mean thickness δ of the boundary layer is such that the Rayleigh number based on δ , Ra_δ say, is just critical ($\approx 10^3$). Thus

$$Nu = H/\delta = (Ra/Ra_\delta)^{1/3} = 0.1Ra^{1/3}, \quad (5.4)$$

in reasonable agreement with experiments [65] using large-Prandtl number fluids. Expressions (5.2–5.4) have been written with the Bénard problem in mind (i.e. with ΔT the temperature difference between the two boundaries and an equal heat flux passing through both boundaries). However, they apply equally well to the more general case in which the heat flux through the top boundary is equal to the sum of the bottom flux and internal heat generation by radioactive decay. In the limit of zero bottom flux, ΔT becomes the temperature drop across the upper thermal boundary layer alone, and (5.3) remains valid.

The expression (5.4) allows one to make crude estimates of Ra and η for the mantle. Using a (poorly constrained) temperature of 3500°C at the base of the mantle [4], at a depth $H = 3000\text{ km}$, an estimate of the overall temperature gradient through the mantle is 1.2 K km^{-1} . The measured temperature gradient near the Earth's surface is of order 20 K km^{-1} . Thus the conducting upper boundary layer, the lithosphere, is very thin compared to H and (5.4) implies that $Nu > 10$, hence $Ra > 10^6$. Inserting the depth and other properties¹ in (5.2) we deduce that the average viscosity is less than $\eta \approx 6 \times 10^{22}\text{ Pas}$. The average viscosity is thus determined by the heat flux and the efficiency of mantle convection. These conclusions, which are based on the assumption of uniform material properties, provide a first approximation to the mantle. As will be seen below, there will be quantitative differences resulting from the temperature- and pressure-dependence of viscosity and other material properties, but the basic conclusions remain unchanged.

The above very robust general arguments show that the existence of a heat flux through a boundary of a convecting region inevitably implies that there will be an unstable conductive boundary layer. However, the two boundary layers at the top and bottom of the Earth's mantle are very different. Because of the strong temperature-dependence of viscosity the upper cold boundary layer will be stiff, and this property will affect the horizontal dimensions of the plates

¹ The values substituted into (5.2) are $\alpha = 3 \times 10^{-5}\text{ K}^{-1}$, $\kappa = 10^{-6}\text{ m}^2\text{s}^{-1}$, $\rho = 3 \times 10^3\text{ kg m}^{-3}$ and $\beta = 0.9\text{ K km}^{-1}$. Remember that by definition β is the difference between the overall temperature gradient over the whole depth, with or without convection, and the adiabatic gradient of 0.3 K km^{-1} . In the convecting region the gradient will of course be much closer to the adiabatic value.

and the behaviour of subducting slabs (Fig.5.1). If the plates are able to move and sink sufficiently rapidly, as is apparently the case for the present oceanic lithosphere, then they represent the unstable boundary layer. On the other hand, it is possible that the surface layer could be so viscous (or strong) that it is stable and does not take part in the underlying convection, instead forming a thick stagnant lid which suppresses heat transport, as suggested to be the case on Venus over the past 500 Myr [54,59]. The behaviour in systems with very viscous, non-convecting upper boundary layers (a problem that is relevant also in the dynamics of cooling magma chambers) has been addressed through laboratory experiments by Davaille & Jaupart [10,11].

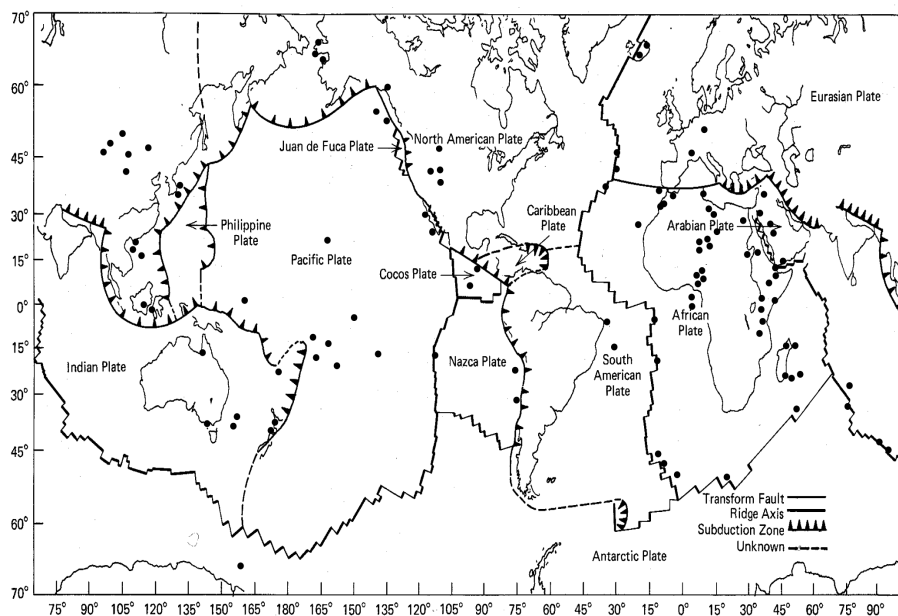


Fig. 5.1. A rendition of the major active boundaries of tectonic plates on Earth, showing the mid-ocean ridges (at divergent boundaries) and subduction zones (at convergent boundaries). Also shown are many of the known "hotspot" plumes that create tracks of volcanism across the moving surface plates. (Adapted from [64])

Since the Earth as a whole, including the core, is cooling, there will be a heat flux out of the core and into the base of the mantle, estimated to be of the order of 10% of the Earth's total surface heat flux (see review by Davies and Richards [17]). The resulting boundary layer of hot, less dense and less viscous material behaves quite differently from the plates produced by surface cooling and may give rise to upwelling plumes (as discussed below). In addition, if there are any internal density interfaces in the mantle separating distinct convecting layers, then boundary layers must form on each side of such interfaces.

Important questions to be answered are: what aspects of the mantle motion lead to topography at its top and bottom boundaries, and can material arising at one boundary layer deliver a sufficient buoyancy force or thermal anomaly to the opposite boundary such that it generates topography by virtue of the buoyant support or the production and eruption of melts? The answer to the latter is clearly ‘yes’ in the case of upwelling plumes, which are believed to be the cause of surface phenomena such as chains of intraplate volcanos [21], uplift of the seafloor surrounding hotspots by the order of 1000m, and eruptions of flood basalts sequences 10km deep and covering millions of square kilometres [53]. It is also clear that temperature (density) differences within the surface boundary layer itself produce surface topography (notably an increase in ocean depth with distance from the spreading centres due to conductive cooling of the lithosphere). At the opposite boundary, the sinking of lithospheric plates may potentially affect the dynamical processes at the core-mantle boundary if they are able to penetrate to sufficient depths.

5.3 Upwelling Thermals and Plumes

We now turn to a discussion of models of specific convective processes in the mantle, starting from the core-mantle boundary (CMB) and working upwards. First we need to consider the implications of a heat flux through the CMB itself. It is also useful to keep in mind the application of these same concepts to convection arising at an internal interface, heated from below.

5.3.1 The Initiation of Convection at the Base of the Mantle

There is a large density difference between the core and the mantle. The best estimates of the temperatures of the outer core and the lowermost mantle (the latter from extrapolation of the upper mantle temperature adiabatically to the CMB), indicate that there is also a large temperature difference (approximately 1300 K; [4]), so that there is a conductive heat flux from the core to the base of the mantle. This temperature drop must occur across a thermal boundary layer. There is direct seismic evidence for a spatially inhomogeneous boundary layer, the so-called D'' layer, above the CMB, which in places is a few hundred kilometers thick [37]. Although there may be significant compositional differences within the D'' layer, it is likely that it also contains the thermal boundary layer.

Because of the strong temperature-dependence of the effective viscosity, there will be a gradient of viscosity through this boundary layer at the bottom of the mantle, with a minimum at the CMB. This reduced viscosity will enhance the flow of the boundary-layer material into any region which has begun to break away from the boundary and convect upwards. An analysis of this lateral flow [60], assuming steady conditions, showed that it will be concentrated in a rheological boundary layer which is much thinner than the thermal boundary layer, and that the lateral flow can be replaced by a slow subsidence of the overlying mantle. Davies [14] combined heat flux estimates with this theory to deduce the

thicknesses of the two boundary layers. As a result of the viscosity variation, the temperature of the rising plume material will be strongly weighted towards the highest temperature in the thermal boundary-layer. However, Griffiths & Campbell [28] noted that the temperature of the plume source material may be much less than that of the core since a thin gravitationally stable conductive layer may persist between a partially miscible or reactive mantle and the much denser core. Such a dense stable layer (not to be confused with either the unstable boundary layer or the D'' layer) will support a large temperature drop without taking part in the boundary layer convection.

In this picture each plume draws boundary layer material from a horizontal area determined only by the separation of unstable convective events. Presumably, if plumes are too far apart, perturbations on the boundary layer between grow to large amplitude and a new plume develops. There is as yet no prediction of this separation distance for large amplitude motions, and hence no prediction of the mean heat and buoyancy flux in each plume. However, we do anticipate from theoretical stability arguments and a variety of experiments, some described here, that the mean separation of plumes will be related to the depth of the boundary layer and not to the overall depth of the convecting layer.

A relevant model here is the so-called Rayleigh–Taylor instability of a thin horizontal layer of fluid beneath a deep fluid of larger density and viscosity. In contrast to convective instability, the effects of heat conduction are removed, the layer depth is prescribed and each layer is uniform. However, the result gives a first estimate of the role of the viscosity contrast and of the horizontal length scale for instability of a convective boundary layer. Figure 5.2 shows a laboratory experiment that exhibits a Rayleigh–Taylor instability, which is a candidate model of instability of the hot boundary layer at the base of the mantle. A lower viscosity layer of dyed fluid lies under a clear deep immiscible fluid of much greater viscosity in a transparent tank. After being left overnight the tank is rapidly inverted and the results photographed. Four or five regularly spaced protrusions were observed shortly after inversion. Within the confines of the box, the protrusions arranged themselves quite uniformly throughout the tank. The dyed fluid had developed long waves which allowed it to buoyantly pass through a clear fluid of much greater viscosity. The wavelength was almost 10 times the depth of the thin layer. The wavelength of maximum growth rate and the exponential time constant for growth have been theoretically and numerically predicted for a number of geometries and boundary conditions for problems like this [1–3, 8, 9, 44–46], [47–50, 56, 70]. Demonstration experiments with putty and non-Newtonian fluids have been extensively photographed and compared to geological formations by Nettleton [41], Parker and McDowell [43] and Ramberg [44, 45, 49]. There was no intercomparison between the laboratory experiments and theory owing to the unknown rheology of the laboratory materials.

In general, if we have two layers of viscous fluid they obey the equations

$$\nabla \cdot \tilde{u} = 0, \quad (5.5)$$

$$(\partial/\partial t - \nu \nabla^2) \tilde{u} = -(1/\rho) \nabla p. \quad (5.6)$$

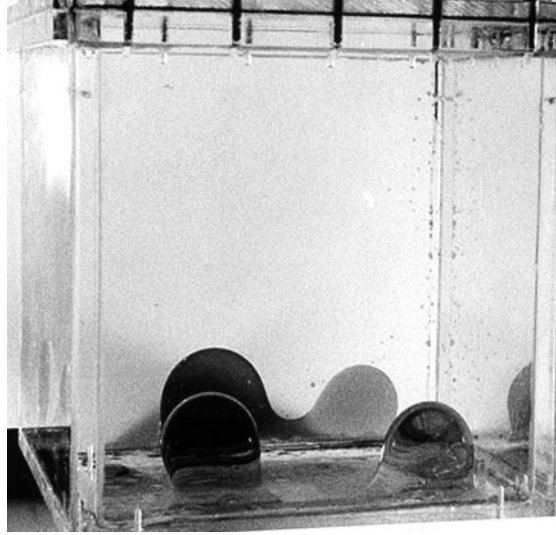


Fig. 5.2. A photograph of a laboratory experiment in which a thin bottom layer of low-viscosity (dyed) fluid is placed beneath a deep upper layer of more viscous fluid and denser clear silicon oil. Viscosity ratio is 43. The bottom layer is initially 5 mm deep and the tank is 18.5 cm^2

Here \tilde{u} is the velocity vector of the fluid, ν is the kinematic viscosity, ρ is density of the mantle and p is the deviation from hydrostatic pressure. These equations can be expected to be valid only for a system in which inertia of the fluid is negligible so that $U_{\max}L/\nu \ll 1$, where L is the largest length scale in the problem (in this case it is either the depth of the layer, the wavelength of a perturbation, or $(\nu^2/g)^{1/3}$, where g is gravity). Since fluid velocity in a viscous medium would be proportional to $g\Delta\rho L^2/\rho\nu_1$, this criterion is easily met in solid Earth geophysics for all the length scales above. We can immediately write down a class of general solutions to these equations in two regions that correspond to the deep mantle and the thin bottom boundary layer respectively. By taking the curl of (5.6) and using (5.5), the equation for the vertical component of velocity w is

$$(\partial/\partial t - \nu\nabla^2)\nabla^2 w = 0. \quad (5.7)$$

This equation can be applied in each region. At the boundaries corresponding to the Earth's surface and the core, $z = h_1, h_2$, we apply zero disturbance boundary conditions. For example, the conditions of zero normal velocity and either zero tangential velocity, or zero tangential stress might be applied. Thus no external forces are driving the fluid at the boundaries. The general expressions for velocity are

$$w_1 = [Ae^{kh_1} + Be^{-kh_1} + Ce^{q_1 h_1} + De^{-q_1 h_1}] f(x, y)e^{nt}, \quad (5.8a)$$

$$w_2 = [Ee^{kh_2} + Fe^{-kh_2} + Ge^{q_2 h_2} + He^{-q_2 h_2}] f(x, y)e^{nt}, \quad (5.8b)$$

where $q_1 = [k^2 + (n/\nu_1)]^{1/2}$, $q_2 = [k^2 + (n/\nu_2)]^{1/2}$ and $\partial^2 f / \partial x^2 + \partial^2 f / \partial y^2 = k^2 f$. To this order, the analysis admits a multiplicity of solutions, each one's growth rate depending on a two-dimensional wave number vector on the horizontal plane. This degeneracy is reduced by finite amplitude effects (Sect. 5.3.2). At the interface, horizontal velocities u, v , vertical velocity w , tangential stresses, and normal stress must be matched. The linearized expressions of these matching conditions are

$$w_1 = w_2, \quad (5.9)$$

$$\frac{\partial w_1}{\partial z} = \frac{\partial w_2}{\partial z}, \quad (5.10)$$

$$\eta_1 \left(\frac{\partial^2}{\partial z^2} + k^2 \right) w_1 = \eta_2 \left(\frac{\partial^2}{\partial z^2} + k^2 \right) w_2, \quad (5.11)$$

$$\begin{aligned} & \left[\rho_1 \frac{\partial}{\partial t} - \eta_1 \left(\frac{\partial^2}{\partial z^2} - k^2 \right) \right] \frac{\partial w_1}{\partial z} + 2k^2 \eta_1 \frac{\partial w_1}{\partial z} = \\ & \left[\rho_2 \frac{\partial}{\partial t} - \eta_2 \left(\frac{\partial^2}{\partial z^2} - k^2 \right) \right] \frac{\partial w_1}{\partial z} + 2k^2 \eta_2 \frac{\partial w_2}{\partial z} + k^2 g (\rho_2 - \rho_1) \hat{z}. \end{aligned} \quad (5.12)$$

Equation (5.12) is a balance of normal stress, where the interface is slightly distorted by an amount $\hat{z}(x, y, t) = z - h$ so that a buoyancy force is produced.

The interface is swept along with the fluid so that

$$\frac{\partial \hat{z}}{\partial t} + u \frac{\partial \hat{z}}{\partial x} + v \frac{\partial \hat{z}}{\partial y} + w \frac{\partial \hat{z}}{\partial z} = 0. \quad (5.13)$$

For small distortions (5.13) can be expanded in a Taylor series

$$\frac{\partial \hat{z}}{\partial t} + u \frac{\partial \hat{z}}{\partial x} + v \frac{\partial \hat{z}}{\partial y} = w(h) + \hat{z} \frac{\partial w}{\partial z} + \dots, \quad (5.14)$$

where velocities and their derivatives are evaluated at the point $z - h = \hat{z} = 0$. For arbitrarily small \hat{z} , (5.14) reduces to

$$\frac{\partial \hat{z}}{\partial t} = w(h). \quad (5.15)$$

Using the solutions given by (5.8a, 5.8b) in (5.9)–(5.12) and using (5.15) we obtain eight linear homogeneous equations for the eight constants. The determinant of these eight equations must be zero.

The limit in which one layer is both thinner and of lower viscosity than the other is particularly relevant to the geophysical context. The wavelength λ of fastest growth is

$$\lambda = 4.6 d \varepsilon^{1/3}, \quad (5.16)$$

and the growth rate is

$$\sigma = 0.232 \left(\frac{g'd}{\nu_2} \right) \varepsilon^{1/3}, \quad (5.17)$$

where $\varepsilon = \nu_2/\nu_1$, ν_1 is kinematic viscosity of the thin layer that is of depth d , ν_2 is viscosity of the infinitely deep fluid above it, and $g' = g\Delta\rho/\rho$ is called the reduced gravity.

The scaling law for a thin layer of relatively low viscosity fluid whereby the wavelength is proportional to the viscosity ratio to the one-third power is very commonly found, although it is not completely universal. The physical interpretation of the $1/3$ power law is that it is more efficient for the low-viscosity fluid to flow large lateral distances up a gradual slope, and to accumulate in massive diapirs, than it is to push straight up through the stiff material with shorter wavelength perturbations. This aspect of the dynamics will be illustrated through the use of a scaling argument here; the complete mathematical derivations are available in the original papers.

Assuming long wavelength compared to depth of the fluid, for a small disturbance the force balance in the thin layer is between the lateral pressure difference p and the viscous drag along the thin sheet, so

$$\frac{p}{\lambda} = \mu_1 \frac{u}{d^2}. \quad (5.18)$$

In the deep fluid above it the force balance is between the pressure, buoyancy and drag from the vertical deformation of the interface so that

$$\frac{p}{\lambda} = \frac{g'\eta}{\lambda} + \mu_2 \frac{w}{\lambda^2}. \quad (5.19)$$

This combines with (5.18) to give

$$\mu_1 \frac{u}{d^2} - \mu_2 \frac{w}{\lambda^2} = \frac{g'\eta}{\lambda}. \quad (5.20)$$

Continuity (conservation of volume flux) is

$$\frac{u}{\lambda} + \frac{w}{d} = 0 \quad (5.21)$$

and the kinematics of the interface is linearized so that

$$\frac{d\eta}{dt} = w. \quad (5.22)$$

Growth will be exponential as $w = w_0 e^{\sigma t}$, where

$$\sigma = \frac{g'}{\nu_2} \left[\frac{\lambda}{\lambda^3/(\varepsilon d)^3 + 1} \right]. \quad (5.23)$$

Maximum growth rate occurs at

$$\frac{\lambda}{d} = 1.26 \varepsilon^{1/3} \quad (5.24)$$

and the maximum growth rate is

$$\sigma = \frac{0.42 g' d}{\nu_2} \varepsilon^{1/3}. \quad (5.25)$$

Thus the wavelength of fastest growth for a thin layer of smaller viscosity is much greater than the depth of the thin layer, but is unrelated to the depth of the overlying very deep layer. The low viscosity fluid accumulates in pockets that push their way into the more viscous fluid assisted by their relatively large volume. One might expect that the hot lower boundary layer of large Rayleigh number convection might exhibit blobs of fluid such as this, with the wavelength again determined by the boundary layer thickness and viscosity contrast as given by (5.16) or (5.24), and not by the overall depth of the convecting layer. We leave predictions for the mantle until Sect. 5.4.

We next consider the large-amplitude structures that arise from boundary layer instability. Experiments in which the buoyancy is due to temperature differences inevitably include the effects of heat conduction and have identified three basic forms of flow that may occur once convection has begun. First, a blob may become detached from the source boundary layer to form an isolated ‘thermal’. Thermals are common in both experiments and numerical solutions of very viscous high-Rayleigh number convection with uniform viscosity, forming when flow sweeps away the feeding conduit or when nearby instabilities on the boundary layer remove the supply of heat. However, it is not clear whether they form in convection with large viscosity variations. Second, the boundary layer instability may lead to an initial transient flow in which the convection forms a mushroom-shaped ‘starting plume’ consisting of a large head and narrow tail, the later acting as a conduit through which fluid continues to be supplied to the head. Third, once a starting plume reaches the opposite boundary a more steady conduit flow may persist. The starting plumes and conduits are likely to be the dominant forms of motion when the viscosity is strongly temperature-dependent. Solutions for each of these forms of convective flow are summarised below.

5.3.2 Isolated “Thermals”

When a volume of buoyant fluid breaks away from the boundary, the resulting structure is known as a ‘thermal’, because of the superficial resemblance to the turbulent atmospheric thermals sought by birds and gliding enthusiasts to provide lift. During ascent of a ‘thermal’ heat can spread and warm up the surrounding cooler material (by conduction in the case of the extremely viscous mantle). However, the warmed material also becomes buoyant and begins to take part in the convection, with the result that the heat is not lost from the convecting region.

Consider first for comparison the case of a bubble of fluid for which the buoyancy is a consequence of an essentially non-diffusive property as in the Rayleigh–Taylor problem above (or a compositional difference in the mantle). In this case the volume of the less dense fluid remains constant. It can be shown that the bubble will become spherical and that the velocity of rise U for a bubble of volume V and diameter D is given by Stokes law:

$$U = \left(\frac{B}{2\pi D\eta_m} \right) f(\eta/\eta_m) , \quad (5.26)$$

where $B = g\Delta\rho V$ is the total buoyancy, η_m is the viscosity far from the bubble and $\Delta\rho$ is the density difference. The factor $f = 1$ when the ratio of viscosities inside and outside the bubble is small and the outer viscosity always has the dominant effect on the rate of ascent.

Theory and laboratory experiments show that the balance of buoyancy and drag (5.26) applies to the rise of thermals in which the density difference $\Delta\rho = \rho_m\alpha\Delta T$ (where ρ_m is the environment density and α is again the coefficient of thermal expansion) is due to a temperature difference ΔT , despite the effects of the conduction of heat [24,25]. Assuming that no heat is lost from a thermal during its ascent, and that α is constant, conservation of heat implies that the buoyancy B (where in this case $B = g\alpha \int \Delta T dV$) is conserved. As heat diffuses outwards into a thin boundary layer of thickness $\delta \approx (\kappa D/U)^{1/2}$ around the thermal, the newly heated layer becomes buoyant (and less viscous) and is drawn into the moving region, so increasing its volume V . The inward volume flux due to this process of ‘thermal entrainment’ is of order $dV/dt \approx UD\delta$ and the overall flow is characterized by a Rayleigh number $Ra_T = B/\kappa\nu_m$, where $\nu_m = \eta_m/\rho_m$ is the kinematic viscosity of the environment.

A solution for self-similar flow can be derived using the above entrainment flux, conservation of buoyancy and the velocity (5.26) [24,25]. We predict the diameter D and height of rise z (above a virtual source at the point $z = 0$, where $D = 0$ and $t = 0$) as functions of time t :

$$D = CRa_T^{1/4}(\kappa t)^{1/2}, \quad (5.27)$$

and

$$z = (f/\pi C)Ra_T^{3/4}(\kappa t)^{1/2}, \quad (5.28)$$

where C is a similarity constant of order unity. The value of C can in principle be predicted using numerical simulations capable of resolving details of the flow within the boundary layer [15,22]. However, it has only been evaluated from experiments (see below). Combining (5.27) and (5.28) shows that the diameter increases linearly with height,

$$D = 2\varepsilon z, \quad (5.29)$$

with a half-angle of spread $\varepsilon = (\pi C^2/2f)Ra_T^{-1/2}$ which is smaller for larger Rayleigh numbers. Hence the thermal enlarges less before reaching a given height for a larger temperature difference or smaller outer viscosity. The requirement that $\delta \ll D$ implies that the analysis applies to cases where $Ra_T \gg 1$. In addition to calculating the size and rate of ascent of a thermal, the above solution can also be used to calculate the shape of particle paths in the fluid, determine which fluid parcels will be entrained, and find the shapes of passive dye markers placed in the flow (Fig. 5.3).

Experiments in which known volumes of heated viscous oil were injected into a cooler environment of the same oil [24] showed that the behaviour was well described by (5.27)–(5.29). Fitting both (5.28) and (5.29) to the data, the similarity constant was found to be $C = 1.0 \pm 0.4$. This laboratory value of C will

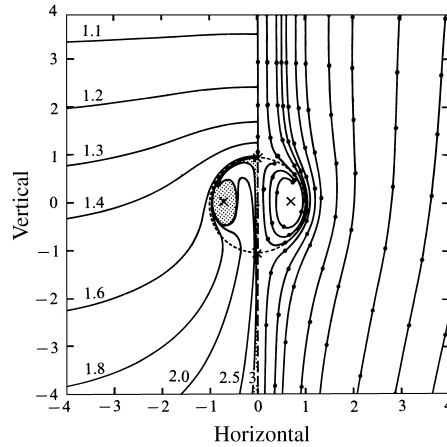


Fig. 5.3. The particle paths (*right*) and deformation of material surfaces (*left*) near a thermal with Rayleigh number $Ra_T \approx 1736$, relative to a frame of reference that is expanding with the diameter of the thermal. All fluid initially lying in a cone above the thermal (and bounded by a dividing streamsurface) is eventually heated and entrained into the thermal. The material surfaces illustrate the large vertical displacement of surrounding fluid that does not form a part of the warm thermal (From [28])

also be applicable to thermals in the mantle, provided the underlying assumptions are satisfied, and allows predictions of ascent speed and plume properties. The predicted shapes into which passive tracers are moulded by the flow compare well with those found in experiments [25]. For example, at $Ra_T > 200$ the internal circulation forms a torus into which all the material originally in the thermal is eventually advected (Fig. 5.3). Since the entrainment process relies on conduction, it is clear that the heat is distributed more widely through the surrounding spherical volume. However, the details of the temperature distribution, which are expected to be of lesser significance for the overall evolution of the flow, are not given by the above solution.

5.3.3 Starting Plumes

When a steady flux of buoyancy is suddenly supplied at the base of a region of viscous fluid (by heating the boundary or by injecting hotter fluid), it produces a nearly spherical volume of buoyant fluid that grows slowly until it becomes large enough to leave the boundary. As the spherical volume rises it remains attached to the source by a cylindrical conduit through which buoyant fluid continues to flow, so increasing the buoyancy and volume of the plume ‘head’ [70]. When the plume fluid has a relatively low viscosity, flow in the conduit (i.e. the hot plume tail) can be rapid, whereas the motion of the ‘head’ remains slow as a result of the larger outer viscosity.

Analysis of a starting plume driven by thermal buoyancy [28] involves only a simple modification of the theoretical treatment for isolated thermals. Conduction round the head again leads to warming and entrainment of surrounding fluid but we must this time take into account the increasing buoyancy in the head with time due to the source flux and the increase in volume due to both the source flux and entrainment. We define an average temperature anomaly for the plume head and, as a result of entrainment and cooling, this will be less than the temperature of the source fluid arriving at the top of the plume head through the axial conduit. The evolution of the plume head is governed by the heat conservation relation

$$V \Delta T = q_0 \Delta T_0 (t - t_0), \quad (5.30)$$

where V is the volume, q_0 is the source volume flux and ΔT_0 is the source temperature anomaly. Along with (5.30), we have the momentum equation (5.26) and the head volume

$$\frac{dV}{dt} \approx q_0 + UD\delta. \quad (5.31)$$

For large times, when entrainment has become important, the solutions for the diameter D , velocity U and temperature anomaly ΔT of the head have the asymptotic forms

$$D \approx z^{3/5}, \quad U \approx z^{1/5}, \quad \Delta T / \Delta T_0 \approx z^{-1}, \quad (5.32)$$

where the constants of proportionality are functions of the plume Rayleigh number, defined in this case by $Ra_p = g\alpha\Delta T_0 q_0^3 / \kappa^4 \nu_m$ [27]. Note that in deriving the above solution we do not need to make any specific assumptions about the form of the profiles of velocity or temperature either in the feeding conduit or in the plume head. The essential assumption is that these profiles remain similar as the flow develops; use of a mean temperature does not require an assumption that the temperature is constant across the plume. But in each of the relations such as (5.32) there is a similarity constant which depends on the real profiles, and which has been evaluated experimentally (see below). In principle it could also be found through finite-element numerical models such as those of Davies [15].

Photographs of a hot starting plume in the interior of a laboratory tank are shown in Fig. 5.4. This plume was produced by injecting hot, dyed syrup at a steady rate into the same (but cold and very viscous) syrup [28]. There was little cooling of the fluid flowing up the conduit until it arrived at the forward stagnation point of the rising head, where it met the resistance of the overlying fluid. There it spread laterally and axisymmetrically as a sheet, facilitating a more efficient heat transfer to a boundary layer in the surrounding fluid, which henceforth became part of the plume head. After the head had ascended a large distance a continuous axisymmetric spiral of dyed material extended inward to a toroidal focus.

Although experiments with continuously fed plumes have gone some way towards determining the coefficient C [23], there are still considerable uncertainties



Fig. 5.4. Photographs of a laboratory starting plume after it has left the source region, enlarges both by continued addition from the source through the conduit and by entrainment, and eventually spreads beneath the free surface. The hot source fluid is dyed. The temperature distribution is not seen. This is one of a series of experiments designed to test the theoretical similarity solution and it illustrates the predicted nature of newly forming mantle plumes. However, for scaling to the mantle it is necessary to use the theory referred to in Sect. 5.3 [28]

in its value (which relates to the rate of incorporation of external fluid into the rising plume head). Departures from self-similarity during the plume ascent in the experiments (due to viscosity changes in the head, a finite volume in the conduit, temporal changes in the head shape, and side-wall effects, all of which are neglected in the simple formulation given here) make it difficult to determine the coefficient to better than a factor of two. However, when the experiments are compared with the solution after small correction terms are included in (5.26, 5.30, 5.31), the result is consistent with that for detached thermals ($C \approx 2$) and is robust enough to allow some firm predictions to be made about the scale and ascent rate of plume heads in the mantle (summarised in Sect. 5.4). The quantitative application to the mantle is also consistent with a range of geophysical data and has been supported by more recent numerical modelling results [12,14,22]. Modifications of the plume behaviour in a mantle of power-law rheology have been computed [67]. These show that plume heads may ascend more rapidly than predicted for a Newtonian mantle, and reach farther into the base of the lithosphere, but that entrainment and head size are not greatly changed.

The distribution of source fluid in the plume head, as seen in Fig. 5.4, does not indicate the temperature distribution, which we can safely assume will be much more smoothly distributed through the bulk of the plume head as a result of

the nature of the ‘thermal entrainment’ process and continued dispersion within the head. The axial conduit and the radial outflow near the top of the head will be almost as hot as the source, and there may be some small remnant temperature maximum near the toroidal focus, whereas the remainder of the source and entrained material in the head will be significantly cooler. Davies [15] and Farnetani & Richards [22] have computed temperature distributions which confirm these ideas, in particular the conclusion that there are only small temperature gradients everywhere, except around the axial conduit and the horizontal outflow at the top of the head. They show that the coupling of advection and conduction is so effective at re-distributing heat between source and entrained material that there is only a small temperature maximum near the toroidal focus of the flow. The hot outflow layer at the top of the plume head and the axial conduit appear as the dominant features in the temperature plots.

5.3.4 Long-lived Plumes

After the head of an (isolated) new plume reaches the top of the layer through which it is rising, and if the source flux is constant, the flow in the trailing conduit delivering material from the source tends toward a steady state. If the surrounding fluid is otherwise at rest, the conduit will be vertical and axisymmetric.

A similarity solution [39] for flow in the vicinity of a steady conduit shows a very strong tendency for the vertical velocity within the conduit to be confined to a thin low-viscosity core, along with a radial balance between the horizontal diffusion of heat out of the conduit and a slow inflow driven by a radial pressure gradient (low pressure in the hotter, lower density conduit). This in effect produces an insulating sheath around the conduit flow. Another similarity solution by Hauri et al. [34] incorporated a wide range of effects of temperature and shear stress on viscosity along with depth-dependent viscosity and thermal expansivity. For a wide range of plausible rheologies, and for buoyancy fluxes of 10^3 – 10^5 N s⁻¹ (see Sect. 5.4.1), vertical velocities in the conduit predicted by this solution range over 0.030–100 myr⁻¹ and conduit radii range over 30–250 km. The extent of dilution by entrainment of surrounding mantle into the conduit flow ranges from under 5% to over 90%, with small buoyancy flux associated with the most entrainment. Most of the entrained material originates from the lower half of the layer traversed by the conduit.

Since mantle plumes are expected to be produced by only a small fraction of the heat flow at the top of the mantle, it is natural to expect the plumes to be strongly influenced by mantle motion driven by movement of tectonic plates and deep subduction (see Sect. 5.5). When there is a larger scale systematic motion in the surroundings, such as a superimposed horizontal shear flow, the conduit will be bent over in the direction of the horizontal flow. The relationship between the shear velocity and the tilt can be simplified to a relation in terms of a vector addition of the horizontal advection velocity and the vertical Stokes velocity of a sphere. For example, with a linear shear profile (in which the horizontal velocity

varies by u_0 over a depth h) and a conduit of fixed diameter D , the formula for deflection $x(z)$ is [52]

$$\frac{x}{h} = \frac{u_0}{2kU} \left(\frac{z}{h}\right)^2, \quad (5.33)$$

where U is given by (5.26) for a sphere with $f = 1$. Laboratory results give $k = 0.54$ [52]. This kinematic theory gives the tilt at the top of the sheared region as

$$\frac{dz}{dx} = \frac{kU}{u_0} \quad (5.34)$$

because the conduit is rotated by an amount that depends on the Stokes rise time of a given conduit element through the depth of the shear zone. If the shear is intense enough to rotate the conduit by more than about 55 degrees from the vertical before it rises out of the region with shear, it will develop an instability [31,52,57]. With instability present, a conduit that is fed steadily at its base will not expel the material steadily at the top of the shear zone, but will develop a chain of new plume heads [69], each rising to a different spot on the surface.

The most obvious application is to the Hawaii-Emperor seamount chain, which not only has been actively producing volcanos for more than 80 Myr, but also experienced a change in plate motion about 40 Myr ago. During this change of motion, the trend of the hot spot track on the Earth's surface changed direction and produced a bend in its path with a radius of less than 200 km, which implies that the upwelling conduit had a small horizontal deviation from the plume source to the surface [31]. Using $u_0 = 0.1 \text{ m yr}^{-1}$, and $U = 0.05 \text{ m/yr}$, corresponding to a density difference of 50 kg m^{-3} , and a (somewhat arbitrarily chosen) conduit radius of 70 km in (5.33)–(5.34) gives a lateral deflection almost exactly equal to the depth of the mantle (which is unknown for the mantle), and the conduit is tilted to 64 degrees. This does not fit the above observation of the abruptness of the bend in the hotspot track unless the shear zone is less than 200 km deep. However, a mantle flow underlain by a return flow gives considerably smaller deflections which do satisfy the observations [31].

Plume conduit solutions based on measured plume buoyancy fluxes (see Sect. 5.4.1), rather than an assumed conduit radius, and which allow for effects of tilting on entrainment have also been constructed [29]. These too predict small horizontal deflections of conduits carrying the relatively large buoyancy flux of the Hawaiian plume. Hence tilt angles for Hawaii are expected to be below the critical angle. Thus strong plumes are expected to experience relatively small deflection and inject a steady flow of mantle material to the base of the lithospheric plates. Weaker plume conduits will be deflected more and thus break up more readily, setting the lower limit to the buoyancy flux that will generate significant effects at the surface. Deep shear zones tend to produce more lateral deflection and thus a greater tilt angle. Shear zones concentrated near the surface tend to produce less lateral deflection and a smaller tilt angle. However, with continuous variation of properties, and with two or three dimensional mantle convection, these simple models must be considered a starting hypothesis at best.

Another consequence of the tilting of plume conduits in a mantle ‘wind’ is enhanced entrainment of the surroundings. While hot material flows upward along the conduit, each part of an inclined thermal-plume conduit must be rising through and continually displacing its surroundings upward if it is to maintain a steady shape, and therefore must contain a circulation in planes normal to the axis of the conduit; the quasi-two-dimensional equivalent of that shown in Fig. 5.3 for the axisymmetric plume head. Surrounding material is again heated in a boundary layer round the rising cylindrical region and is drawn into it, so increasing the volume flux in the conduit. The source material is concentrated into two cores, leaving a central strip which is relatively free of source fluid [53]. The solutions referred to above for the thermal conduit flow [29] predict that entrainment has a much greater effect on bent-over plumes when the temperature-dependent viscosity in the plume is allowed to increase with distance from the source due to entrainment and cooling, since in order to cope with the imposed buoyancy flux the diameter of the conduit must then increase (with height) as the plume cools. The solution also predicts that, as for starting plumes, the behaviour is a function of the plume Rayleigh number $Ra_p = g\alpha\Delta T_0 q_0^3 / \kappa^4 \nu_m$, where q_0 is the source volume flux. Plumes with larger buoyancy fluxes will be less tilted and entrain a volume flux from the surroundings that is smaller relative to the source volume flux (i.e. they will be less diluted).

5.3.5 Surface Uplift

Experiments have also been used to help predict the surface topography generated by the arrival of a plume head beneath the surface of a convecting fluid or the continued upwelling of a plume conduit. For example, capacitance [42] and optical interferometric observations [31] give the maximum surface uplift and the maximum rate of uplift over a rising spherical diapir

$$h_{\max} = 0.27(\Delta\rho/\rho_m)D_0, \quad (5.35a)$$

$$v_{\max} = 0.16(\Delta\rho/\rho_m)U_0, \quad (5.35b)$$

where $\Delta\rho$ is the density anomaly, ρ_m is the surrounding density and D_0 and U_0 are the diameter and velocity of the diapir when it is far from the surface. The diapir or plume head spreads horizontally as it approaches closer than one radius from the surface, but the rate of spreading decreases as $D \sim t^{1/5}$, so that further spreading is very slow after the horizontal radius has doubled [30]. This result is in agreement with theoretical scaling laws for the radial spreading of a low-viscosity blob into a high-viscosity fluid. The surface reaches a maximum uplift after which it slowly subsides and the width of the surface swell increases. During this collapse a thin layer of more dense outer fluid remains above the top of the plume and thins (according to a $t^{-1/2}$ law) to around $0.1D_0$ when the plume diameter has doubled. In the laboratory experiments, this layer becomes gravitationally unstable at a time $Ut/D_0 \approx 10$ after maximum uplift is reached, and overturning with the underlying plume fluid leads to either axisymmetric convective flow or to irregular three-dimensional convection. This smaller scale

of convection is able to more rapidly continue the release of potential energy and enable the plume fluid to penetrate closer to the surface.

Similar behaviour is expected where a continuing conduit flow impinges beneath migrating oceanic crust. In this case, uplift of the surface occurs upstream of and above the upwelling flow in the conduit, where buoyancy is being added to the mantle beneath the crust, leading to the seafloor swell. Subsidence of the swell and its associated volcanic island chain occurs with age downstream of the conduit location, where horizontal spreading flow of the hot plume material beneath the lithosphere proceeds to slowly redistribute the buoyancy across an increasingly broad region.

5.4 Mantle Plumes and Surface Topography

In order to apply the theoretical, computational and laboratory results discussed above to predict plume velocities and sizes in the mantle, one first needs to make realistic estimates from geophysical data of the material properties (in particular the viscosity), and also of the temperature anomaly and heat flux at the source.

5.4.1 Plume Fluxes from Hotspot Tracks

One of the most important inputs to quantitative predictions for plumes in the mantle is the boundary condition on temperature or heat flux, or both, at the base. The plume heat flux $F_H = q_0 \rho c_p \Delta T_0$ (or, more precisely, the plume buoyancy flux $F_B = g \alpha F_H / c_p$, where c_p is the specific heat capacity and q_0 is again the source volume flux, as in (5.30)) has the primary control on the plume flow. The temperature anomaly plays a lesser role through its influence on the viscosity difference and partial melting. The range of plume fluxes to be found in a convecting fluid with temperature-dependent viscosity is not yet understood: it will be related to the plume spacing. However, we can understand individual plumes by considering a single plume in isolation from other plumes and lateral boundaries, and specifying both a source temperature anomaly and buoyancy flux³ based on geophysical constraints.

We begin by applying the results for Rayleigh–Taylor instability of a thin layer to the bottom boundary layer of the mantle in order to estimate the separation of plumes. Assuming the unstable layer is 50 to 100 km thick, and a viscosity contrast $\varepsilon \approx 10^3$ the wavelength (5.16) is of order 600–1200 km. This wavelength is consistent with the separation of volcanic hotspots within the Pacific Plate, where the separation is significantly smaller than the depth of the mantle. The result indicates a strong effect of the viscosity contrast. The analysis

³ In most computer models of a convecting layer, only one of these is imposed, since the other is then determined by the coupling of conduction and convection of the bottom boundary layer. In numerical experiments [15,22] this was done by applying a temperature anomaly over a finite area of the bottom boundary. In the laboratory experiments described above the temperature anomaly and source mass flux are prescribed.

is expected to apply to the onset of instability on the boundary layer between existing plumes, where new plumes may be initiated. However, it should be remembered that the linear stability analysis does not necessarily predict well the separation of well-established plume conduits or the effects of large-scale convective flow driven by sinking of the cold surface boundary layer, which may advect plumes into regions of convergence of the large scale flow.

Estimates of the plume buoyancy and heat fluxes in the mantle have been made using observations of the surface effects of long-lived plumes in oceanic settings, where the crust exerts relatively little masking compared to that of thicker continental crust [12,58]. The size of the hotspot swell can be combined with the velocity of the plate over the hotspot to obtain the rate of production of anomalous topography, from which we infer the buoyancy flux carried by the plume. For example, the existence of the Hawaiian swell, about 1000 km wide and 1 km high, propagating across the Pacific plate at about 100 mm yr^{-1} , implies a buoyancy (or mass-deficit flux) in the plume of $7.3 \times 10^3 \text{ kg s}^{-1}$. This mass-deficit flux is actually $\alpha\Delta TQ$, where Q and ΔT are the mass flux and temperature difference at any depth. This is related to the more physically meaningful buoyancy and heat fluxes through $F_B = g(\alpha\Delta TQ)$, and $F_H = (c_p/\alpha)(\alpha\Delta TQ)$, respectively. For the Hawaiian plume $F_B \approx 8 \times 10^4 \text{ N s}^{-1}$ and $F_H \approx 3 \times 10^{11} \text{ W}$. The distribution of plume mass-deficit fluxes (calculated by Sleep [58] and Davies [12] for 35 oceanic hotspots) therefore imply the buoyancy fluxes as plotted in Fig. 5.5 [32]. Although there are many uncertainties in such estimates, they do indicate that plumes carry a range of fluxes, and that the distribution is (logarithmically) centred about 10^4 N s^{-1} .

An estimate of the volume or mass flux requires independent knowledge of the temperature anomaly, which is usually obtained from the petrology of erupted melts. However, the mass flux is not a conserved quantity in that it, like the temperature, may vary with height along a plume. Nor is the mass flux well-defined: on the one hand, the mass flux of *hot material* near the top of the plume (the flux that is relevant to melt production) for the Hawaiian example becomes $Q_{\text{top}} = F_B/(g\alpha\Delta T) \approx 3 \times 10^5 \text{ kg s}^{-1}$ (assuming an average temperature anomaly of 100 C and no large scale shearing); on the other hand, the movement of the lithospheric plate over the plume implies, as we have already explained, that upper mantle is continuously being displaced by the plume and that there must be a vertical mass flux in the cooler surroundings. The upward mass flux relevant to overall motion and stirring in the mantle is then made up of both the slow broad motion of the surroundings (associated with the Stokes ascent of the plume conduit in the presence of plate migration), and the Poiseuille-like pipe flow (at relatively large velocities) of low-viscosity material upward through the narrow conduit. Unpublished experiments (by RG) with stirring when a plume conduit passes through a larger-scale overturning convection cell will not be discussed here but show how the former of these two transport components may be dominant and lead to a large vertical transport of the surroundings up toward the surface, as well as to disturbance of particle paths in the large scale cell.

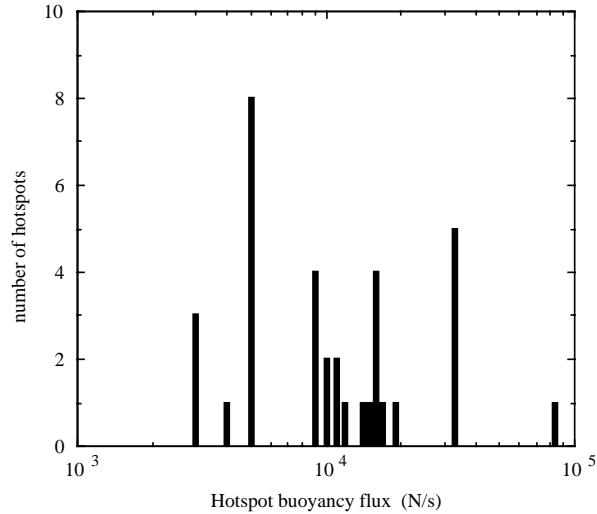


Fig. 5.5. Plume buoyancy fluxes, adapted from Sleep's [58] estimates of the fluxes for 35 oceanic hotspots [29,32]. The buoyancy flux is Sleep's 'mass exchange flux' multiplied by g

5.4.2 New Plumes and Flood Basalts

Predictions can be made for new plume heads by assuming that the rate of supply of buoyancy from the source boundary layer during this early stage in the life of a plume falls in the same range as the buoyancy fluxes derived for currently active hotspot tracks. In that case a mantle viscosity of 10^{22} Pas implies that heads will grow as large as 400–600 km in diameter at the core–mantle boundary before their ascent speed is large enough to cause them to break away. Application of the complete form of (5.32) [28] to the ensuing motions leads to the prediction of a further doubling of the diameter (and an increase of volume by an order of magnitude) as the plume heads ascend through 2800 km. Thus plume heads that reach the lithosphere while still receiving a constant influx from their source region are predicted to be extremely large: 800–1200 km in diameter. They will also have incorporated a volume of lower mantle material comparable with the total volume supplied from the source, though the ratio of these two volumes depends on the source flux. The head size, however, is insensitive to the flux. The diameter D is instead dependent primarily on the mantle viscosity ($D \approx \eta_m^{1/5}$).

As a plume head approaches the upper boundary (the free surface in the laboratory tank, or the stiff lithosphere of the Earth) it must flatten and spread. Thus a spherical head, predicted to be of order 1000 km in diameter, should produce a pancake-shaped thermal anomaly about 2000 km across at the base of the lithosphere. It should be remembered that the dimension given by the model is the diameter of the equivalent sphere that would contain the plume head buoy-

ancy at an average temperature, and that some of the head will be much cooler while the top of the head will contain the hottest material supplied from the source via the conduit. Similar head sizes and ascent times are predicted by numerical experiments simulating mantle conditions [15,22], and the chronology, tectonics and geochemistry of flood basalt provinces, believed to be attributable to plume heads, are consistent with the 1000–2000km scale. Furthermore, continental flood volcanism is known to be characterised by a sudden onset, with most of the magmas erupted within a short period of 1 to 3 Myr [53] and over a roughly equant region 2000–2500km across, followed by slow subsidence. Use of these comparisons to argue in the opposite direction provides evidence that plume heads responsible for the major flood basalts had dimensions consistent only with an origin deep in the lower mantle and therefore most probably in the thermal boundary layer at the CMB.

5.5 The Upper Boundary Layer

We turn now to the cooled upper boundary, and the generation of the primary motions of mantle convection. The total heat flux at the Earth's surface, apparently an order of magnitude greater than the flux carried by hot plumes, is largely due to loss of the heat generated by radioactive decay. That is, the mantle may be regarded as a layer of viscous fluid, largely internally heated, and cooled from above.

Early notions about mantle convection regarded plate tectonics as the surface reaction to an underlying pattern of convection occurring especially in the upper mantle. This view required the plates to be dragged along by a faster motion beneath. When the observations (Fig. 5.1) were compared with laboratory studies with this picture in mind, it was puzzling that the inferred convection cells are so much wider than their depth (often presumed to be that of the upper mantle), and this led to many investigations of the effect of variable fluid properties and different boundary conditions on the aspect ratio. A more consistent view is that the buoyancy forces acting on the colder, denser plates are the primary driving mechanism of convection, at least under the present tectonic regime, so subduction and descent of lithospheric slabs is an active part of convection, not a reaction to it. The plates are the upper thermal boundary layer. Those earlier questions about the horizontal scale are then readily answered by 1) considering that the convection may penetrate the full (2900km) depth of the mantle and 2) noting that the strength of the lithosphere (which can yield and break only at stresses greater than a few hundred MPa) can inhibit the initiation of subduction and thus increase the horizontal scale of convection cells. In this view cold material can break away from the upper boundary only at plate boundaries where one plate may slide under the other. Near mid-ocean ridges there is a compensating, passive ascending flow – this upwelling limb of the convection is not a hot active plume. Thus much of the structure of convection in the mantle is organized by the pattern of the plates, though the prediction of the criteria for

formation and size of these plates, and for the initiation of subduction, remains a major theoretical challenge.

The most significant topographic characteristics of plate convection are the deep ocean trenches (up to 5000 m below the mean sea floor) at the subduction zones and the mid-ocean ridges (standing 3000 m above the plate spreading centres). The trenches are clearly the effect of the presence below the surface of a larger mass of cold dense lithosphere (this negative buoyancy will pull down the surface even in the absence of motion) as well as the downward motion of the slab. The topographic high above the spreading centres and its steady fall-off with distance from the ridge have been shown to be a simple consequence of conductive cooling of the oceanic lithosphere and thermal contraction while remaining in isostatic balance with the whole of the seafloor [18]. The plate motion, driven by surface cooling and subduction, produces a pressure gradient that “pulls” warm mantle material up to the surface at the spreading centre. Close to the ocean floor this material proceeds to cool and hence increases its density as it moves away from the centre. This produces an additional ocean depth Δd which can be found from the buoyancy balance $g\Delta\rho\Delta d = g\rho_m\alpha\Delta Tz$, where $z = 2(\kappa t)^{1/2}$ is the conductive thickness of the lithosphere, κ is the thermal diffusivity of the lithosphere, t is the age of any section of the lithosphere, ρ_m is the density of the mantle, ΔT is the average temperature of the lithosphere relative to the surface and $\Delta\rho$ is the density difference between the mantle and seawater. The result is $\Delta d = 2\alpha\Delta T(\rho_m/\Delta\rho)(\kappa t)^{1/2}$, which predicts about 3000 m relief between old seafloor (100 Myr old and 100 km thick) and the ridge crest (using $\alpha = 3 \times 10^{-5} \text{ }^\circ\text{C}^{-1}$, $\rho_m = 3,300 \text{ kg m}^{-3}$, $\Delta T = 650 \text{ }^\circ\text{C}$). This square root of seafloor age relation explains most of the measured topography, which is therefore consistent with a predominantly internally-heated mantle undergoing convection due to surface cooling, and with a passive upwelling at normal mantle temperature under the ridge.

5.6 Synopsis

The dominant large-scale morphology of the earth’s surface is a direct consequence of the dynamics of thermal convection in the Earth’s solid mantle. The two major topographic features of the ocean floor, ocean trenches and mid-ocean ridges, represent active boundaries of the tectonic plates where the upper thermal boundary layer of the mantle convection system is foundering and sinking into the interior or just beginning its thermal development, respectively. The topography is dynamic, being produced by buoyancy differences within the lithosphere. We have not discussed continents and their major mountain belts, however these too are directly produced by mantle convection through plate collisions (either of continent with continent, such as the formation of the Himalaya by the collision of the Indian sub-continent with the Eurasian continent and the formation of the European Alps by the collision of Africa with Europe, or of oceanic plate and continent, as in the Sierra Ranges and Andes of the Americas). Looking at more isolated structures, but still at a large scale, continental

flood basalt provinces (such as the Deccan Traps of India) and oceanic plateaux (such as the Ontong-Java plateau in the Pacific), each of order 1000–2000 km across and 1000–2000 m high, and volcanic ('hotspot') tracks such as ocean island chains and their accompanying, broader seafloor swells, are all thought to be generated by the buoyancy of hot upwelling plumes. These most probably ascending from the core-mantle boundary. Plumes are also thought to have been the cause of continental rifting and the initiation of the opening of new ocean basins [35,68]. The role of mantle convection in the generation of surface morphology has meant that knowledge of the surface topography has provided important evidence about the way in which the mantle works. This topography strongly influences ocean and atmosphere circulation patterns. It also acts as major drainage highs, which are eroded during and after their formation, and drainage lows, which capture vast amounts of sediment.

References

1. H. Berner, H. Ramberg, O. Stephansson: *Tectonophysics* **15**, 197 (1972)
2. M.A. Biot, H. Ode: *Geophysics* **30**, 213 (1965)
3. M.A. Biot: *Geophysics* **30**, 153 (1966)
4. R. Boehler: *Nature* **363**, 534 (1993)
5. B.A. Buffet, H.E. Huppert, J.R. Lister, A.W. Woods: *J. Geophys. Res.* **101**, 7989 (1996)
6. I.H. Campbell, R.W. Griffiths: *Earth Planet. Sci. Lett.* **99**, 79 (1990)
7. I.H. Campbell, R.W. Griffiths: *J. Geol.* **92**, 497 (1992)
8. S. Chandrasekhar: *Hydrodynamics and Hydromagnetic Stability* (Oxford University Press, New York 1961)
9. Z.F. Danes: *Geophysics* **29**, 414 (1964)
10. A. Davaille, C. Jaupart: *J. Fluid Mech.* **253**, 141 (1993)
11. A. Davaille, C. Jaupart: *J. Geophys. Res.* **99**, 19,853 (1994)
12. G.F. Davies: *J. Geophys. Res.* **93**, 10,467 (1988)
13. G.F. Davies: *J. Geophys. Res.* **93**, 10,451 (1988)
14. G.F. Davies: *Geophys. J. Int.* **115**, 132 (1993)
15. G.F. Davies: *Earth Planet. Sci. Lett.* **133**, 507 (1995)
16. G.F. Davies, M. Gurnis: *Geophys. J. Roy. Astr. Soc.* **85**, 523 (1986)
17. G.F. Davies, M.A. Richards: *Geophys. J. Geol.* **100**, 151 (1992)
18. G.F. Davies: *Dynamic Earth: Plates, Plumes and Mantle Convection* (Cambridge University Press, Cambridge 1999)
19. M.B. Dobrin: *Eos Trans. AGU* **22**, 528 (1941)
20. M.R. Drury, J.D. FitzGerald: 'Mantle Rheology: Insights from laboratory studies of deformation and phase transformation'. In: *The Earth's Mantle: Composition, Structure and Evolution*, ed. by I. Jackson (Cambridge University Press, New York 1998) pp. 503–559
21. R.A. Duncan, M.A. Richards: *Rev. Geophys.* **29**, 31 (1991)
22. C. Farnetani, M.A. Richards: *Earth Planet. Sci. Lett.* **136**, 251 (1995)
23. M.F. Fitzpatrick: The dynamics of viscous thermal plumes in the Earth's mantle. Honours Thesis, The Australian National University (1991)
24. R.W. Griffiths: *J. Fluid Mech.* **166**, 115 (1986)
25. R.W. Griffiths: *J. Fluid Mech.* **166**, 139 (1986)

26. R.W. Griffiths: *Earth Planet. Sci. Lett.* **78**, 435 (1986)
27. R.W. Griffiths: *Phys. Fluids, A* **3**, 1233 (1991)
28. R.W. Griffiths, I.H. Campbell: *Earth Planet. Sci. Lett.* **99**, 66 (1990)
29. R.W. Griffiths, I.H. Campbell: *Earth Planet. Sci. Lett.* **103**, 214 (1991)
30. R.W. Griffiths, I.H. Campbell: *J. Geophys. Res.* **96**, 18, 295 (1991)
31. R.W. Griffiths, M.A. Richards: *Geophys. Res. Lett.* **16**, 437 (1989)
32. R.W. Griffiths, J.S. Turner: 'Understanding mantle dynamics through mathematical models and laboratory experiments'. In: *The Earth's Mantle: Composition, Structure and Evolution*, ed. by I. Jackson (Cambridge University Press, New York 1998) pp. 191–227
33. R.W. Griffiths, M. Gurnis, G. Eitelberg: *Geophys. J.* **96**, 1 (1989)
34. E.H. Hauri, J.A. Whitehead, S.R. Hart: *J. Geophys. Res.* **99**, 24275 (1994)
35. R.I. Hill, I.H. Campbell, G.F. Davies, R.W. Griffiths: *Science* **256**, 186 (1992)
36. L.N. Howard: 'Convection at high Rayleigh number'. In: *Proc. 11th Int. Congress Applied Mechanics, Munich 1964*, ed. by H. Görtler (Springer-Verlag, Berlin) pp. 1109–1115
37. B.L.N. Kennett, R. van der Hilst: 'Seismic structure of the mantle: From subduction zone to craton'. In: *The Earth's Mantle: Composition, Structure and Evolution*, ed. by I. Jackson (Cambridge University Press, New York 1998) pp. 381–404
38. K. Lambeck, P. Johnston: 'The viscosity of the mantle: Evidence from analyses of glacial-rebound phenomena'. In: *The Earth's Mantle: Composition, Structure and Evolution*, ed. by I. Jackson (Cambridge University Press, New York 1998) pp. 461–502
39. D.E. Loper, F.D. Stacey: *Phys. Earth Planet. Interiors* **33**, 304 (1983)
40. W.J. Morgan: *Nature* **230**, 42 (1971)
41. L.L. Nettleton: *Amer. Ass. Petrol. Geol. Bull.* **18**, 1175 (1934)
42. P.L. Olson, I.S. Nam: *J. Geophys. Res.* **91**, 7181 (1986)
43. T.J. Parker, A.N. McDowell: *Amer. Ass. Petrol. Geol. Bull.* **39**, 2384 (1955)
44. H. Ramberg: *Bull. Geol. Inst. Univ. Uppsala* **42**, 1 (1963)
45. H. Ramberg: *Geophys. J.* **14**, 307 (1967)
46. H. Ramberg: *Phys. Earth Planet. Interiors* **1**, 63 (1968)
47. H. Ramberg: *Phys. Earth Planet. Interiors* **1**, 427 (1968)
48. H. Ramberg: *Phys. Earth Planet. Interiors* **5**, 45 (1968)
49. H. Ramberg: *Geol. J. Spec. Issue* **2**, 261 (1970)
50. Lord Rayleigh: *Scientific papers*, ii (Cambridge University Press, Cambridge 1900), 200–207
51. M.A. Richards, R.A. Duncan, V.E. Courtillot: *Science* **246**, 103 (1989)
52. M.A. Richards, R.W. Griffiths: *Geophys. J.* **94**, 367 (1988)
53. M.A. Richards, R.W. Griffiths: *Nature* **342**, 900 (1988)
54. G.G. Schaber, R.G. Strom, H.J. Moore, L.A. Soderblom, R.L. Kirk, D.J. Dawson, L.R. Gaddis, J.M. Boyce, J. Russell: *J. Geophys. Res.* **97**, 13,257 (1992)
55. J.G. Sclater, J. Francheteau: *Geophys. J. Royal. Astron. Soc.* **20**, 509 (1970)
56. F. Selig: *Geophysics* **30**, 633 (1965)
57. J.N. Skilbeck, J.A. Whitehead: *Nature* **272**, 499 (1978)
58. N.H. Sleep: *J. Geophys. Res.* **95**, 6715 (1990)
59. V.S. Solomatov, L.N. Moresi: *J. Geophys. Res.* **101**, 4737 (1996)
60. F.W. Stacey, D.E. Loper: *Phys. Earth Planet. Interiors* **33**, 45 (1983)
61. D.J. Stevenson, J.S. Turner: 'Fluid models of mantle convection.' In: *The Earth: Its origin, structure and evolution*, ed. by M.W. McElhinny (Academic Press, London 1979) pp.227–263

62. D.C. Tozer: *Phil. Trans. R. Soc. A* **258**, 252 (1965)
63. D.L. Turcotte, E.R. Oxburgh: *Ann. Rev. Fluid Mech.* **4**, 252 (1972)
64. D.L. Turcotte, G. Schubert: *Geodynamics applications of continuum physics to geological problems* (John Wiley and Son, New York 1982)
65. J.S. Turner: *Buoyancy Effects in Fluids* (Cambridge University Press, Cambridge 1973)
66. J.S. Turner: *Earth Planet. Sci. Lett.* **17**, 369 (1973)
67. R. Weinberg, Y.Y. Podladchikov: *J. Structural Geol.* **17**, 1183 (1995)
68. R. White, D. McKenzie: *J. Geophys. Res.* **94**, 7685 (1989)
69. J.A. Whitehead: *Ann. Rev. Fluid Mech.* **20**, 369 (1988)
70. J.A. Whitehead, P.S. Luther: *J. Geophys. Res.* **80**, 705 (1975)